ISSN: 2277-3754
ISO 9001:2008 Certified
International Journal of Engineering and Innovative Technology (IJEIT)
Volume 7, Issue 6, December 2017

Finite Element Investigation of RC Cantilever Slabs Strengthened with Different Systems

Aymen Hussien Khalil, Ashraf Mohammed Heniegal, Bassam Abdelsalam
Structural Engineering, Ain Shams University, Cairo, Egypt
Civil and Architectural Constructions Department, Suez University, Suez, Egypt
Civil and Architectural Constructions Department, Suez University, Suez, Egypt

Abstract*—This paper presents a finite element (FE) model for predicting the behavior of a reinforced concrete cantilever slabs strengthened with different techniques. Seven FE models were developed based on experimental test. The experimental program included seven cantilever slabs strengthened with RC jacket, GFRP layers and steel plates then tested with concentrated load to failure. Cracking loads, yield loads and failure loads were used as bench mark for comparison between experimental and FE results. The developed FE models have exact geometry, nonlinear material properties and boundary conditions to that of the experimental specimens. It is concluded that the FE results gave the best correlation with the experimental results.

***Index Terms*— Cantilever slabs, finite element model, GFRP layers, strengthened.**

I. INTRODUCTION

The strengthening and rehabilitation of existing structures is now a challenging problem facing civil engineers all over the world. Many reinforced concrete (RC) structures constructed in the past are no longer considered safe due to increase in live loads; change in design codes and specifications or due to the effect of carbonation, corrosion or chloride attacks [1]. With the development of powerful computer platforms, numerical models have become widely available and useful in simulating the behavior of structural members under various loading, geometrical, and material configurations. Numerical models can be used as an alternative method when the geometry, loading configuration, or material behavior of a member are too complex to be solved by closed-form analytical models. Also, numerical tools can supplement experimental testing and assist in exploring effects of various parameters, left out in the experimental program, due to time, apparatus or cost limitations. Several methods, namely finite element (FE), finite difference, boundary element, are available. The FE method is the most widely practiced method [2]-[4]. FRP is particularly suitable for structural repair and rehabilitation of reinforced and prestressed concrete elements. The low weight reduces both the duration and cost of construction since heavy equipment is not needed for the rehabilitation. The composites can be applied as a thin plate or layer by layer. The fiber reinforced polymers (FRP) are a composite material which are used for many years to retrofitting various elements in construction. Moreover, the properties of the composite material with epoxy resin have advantages such as resistance to corrosion, high tensile strength and reasonable stiffness. Consequently, causing improvement in the behavior of the structure elements [5].

II. SUMMARY OF EXPERIMENTAL PROGRAM

The experimental program consisted of testing seven specimens for evaluation the efficiency of the strengthening techniques proposed for reinforced concrete cantilever slabs. All specimens have the same dimensions 140 mm thickness, 600 mm width and 2500 mm length and the same steel reinforcement. Fig. 1 shows the concrete dimensions and the details of reinforcement for each tested sample. The repaired and strengthened elements consisted of six cantilever slabs which were divided into three groups. In the first group, reinforced concrete jackets with and without shear connector bars were used. The second group had two samples strengthened using two layers of GFRP laminates (covering 60% and 90% of the cantilever length).

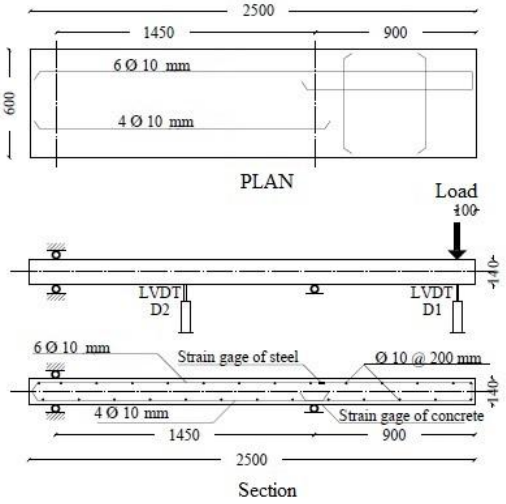

Fig. 1: Dimensions of slabs and details of reinforcement

The third group had two slabs strengthened with two steel plate (one of them glued by epoxy and the other one affixed using steel expansion bolts). The length of steel plates covered about 90% of cantilever length. The cantilever elements were loaded up to 40% of the ultimate load of control cantilever slab. Then, repairing the cracks with epoxy injection and strengthening with different techniques were applied. The test specimens were re-loaded to failure. The descriptions of the cantilever slab are tabulated in Table 1.

ISSN: 2277-3754
ISO 9001:2008 Certified
International Journal of Engineering and Innovative Technology (IJEIT)
Volume 7, Issue 6, December 2017

Table 1: Descriptions of the cantilever slabs

Slabs	Descriptions	Dimensions (mm)
S-1	Control slab	140×600×2500
S-2	RC jacket without shear connector bars	210×600×2570
S-3	RC jacket with shear connector bars	210×600×2570
S-4	GFRP covering 60% of cantilever length	Two layers of GFRP 1.10×100×2030
S-5	GFRP covering 90% of cantilever length	Two layers of GFRP 1.10×100×2270
S-6	Steel plates using epoxy resin 90% of cantilever length	10×100×2270
S-7	Steel plates using expansion bolts 90% of cantilever length	10×100×2270

The materials used in this study are ordinary Portland cement (CEM I 42.5 N) for all cantilever slabs and (CEM I 42.5 R) for addition concrete layer of enlargement cantilever slabs according to Egyptian Standard Specifications ES 4756-1/2013 [6]. Natural sand and crushed stone as fine and coarse aggregates were used according to ES 1109/2002 [7] and ECP 203-2009 [8]. The set-up of cantilever elements arranged in the concrete laboratory. The applied load was applied at a distance of 800 mm from the roller support and the distance between the fixed and the roller supports was 1450 mm. Two strain gauges were glued by epoxy on the bottom surface near to the roller support to measure the compressive strain of concrete. Six Linear Variable Differential Transformers (LVDTs) have been used to determine the deflections of cantilever slabs at two points which distributed to three LVDTs under the applied load and three LVDTs at mid-span between the supports.

III. MATERIAL MODEL

The material model used in the ANSYS R15.0 software [9] is tabulated from table 2.

A. Concrete material model

Two concrete grades were used in this study, the first concrete grade is used for all specimens. The second concrete grade is casting as additional concrete layer for strengthening by enlargement cantilever slab. Concrete is assumed as linear isotropic material, and the stress-strain curve of concrete material is presenting from fig. 3. The young's modulus and Poisson's ratio are taken with 26600 N/mm^2 and 0.2 while for additional concrete layer are taken by 27000 N/mm^2 and 0.2 respectively according to the Egyptian Code [8]. The stress-strain curve is divided into two parts. The first part show the linear elastic zone. The second part shows the elastic-plastic zone at the maximum compressive stress of concrete material. The uniaxial crushing stress is equal to 34 N/mm^2 while for additional concrete layer is 38 N/mm^2 according to average cubes at loading age. The uniaxial cracking stress is assumed by 4.5 N/mm^2 for both concrete grades.

B. Steel reinforcement model

An elastic material is assumed for all steel reinforcement bars. Bilinear isotropic hardening stress–strain relationship was used for steel bars. The elastic-plastic behavior of the steel reinforcement bars and was 200000 N/mm^2 for Young's modulus and 0.3 for the Poisson's ratio. The yield stress and the tangent modulus are 552 N/mm^2 and 1500 respectively. Similar bilinear stress-strain relationship was adopted for the steel plate material as shown from fig. 4.

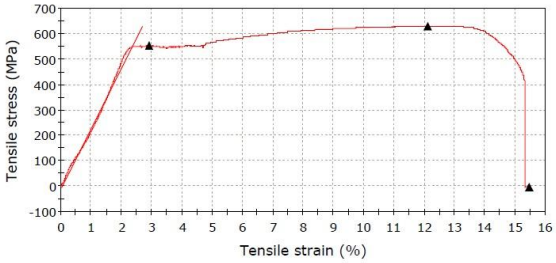

Fig. 2: Stress-strain curve for steel reinforcement bar

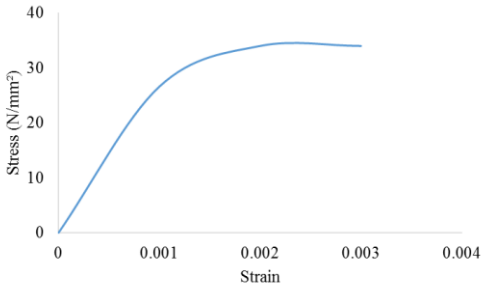

Fig. 3: Stress-strain curve for concrete

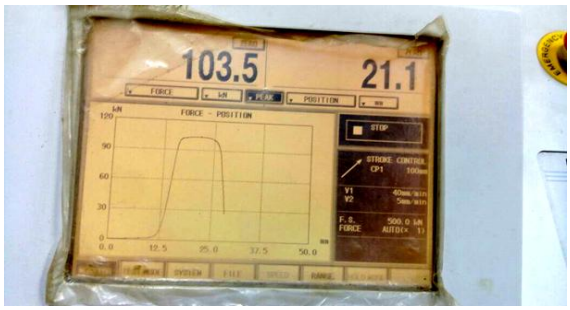

Fig. 4: Stress-strain of steel plate

C. Glass Fiber Reinforced Polymer (GFRP) model

An isotropic linear elastic behavior is assigned for GFRP laminates and for adhesives. A failure criteria is defined for each component. The linear response is assumed to continue until the tensile strength is reached, and beyond that a complete tensile failure is assumed. A poisson's ratio of 0.3 was assigned for GFRP sheets and epoxy resin.

Table 2: Materials simulation with elements type

Elements type	Modeled parts
SOLID65	Concrete
LINK180	Steel bars
SOLID45	Steel supports
SOLID185	GFRP layers or steel plates
CONTA174	Contact element between concrete surface and strips

ISSN: 2277-3754
ISO 9001:2008 Certified
International Journal of Engineering and Innovative Technology (IJEIT)
Volume 7, Issue 6, December 2017

IV. LOADING SCHEME AND BOUNDARY CONDITIONS

The boundary conditions of the tested cantilever slabs are continuous slab from one direction. The slab models are rested on two supports, hinge support at the end of slab and roller support at 1.45 m from the hinge support. The load scheme is concentrated load and located at the end point of cantilever slab and at 0.90 m from roller support.

V. FINITE ELEMENT MESHING

Along the length of the cantilever slab, a mesh size is 25 mm. The concrete, steel reinforcement bars, GFRP laminates and supports are meshing as shown from fig. 5 to fig. 8.

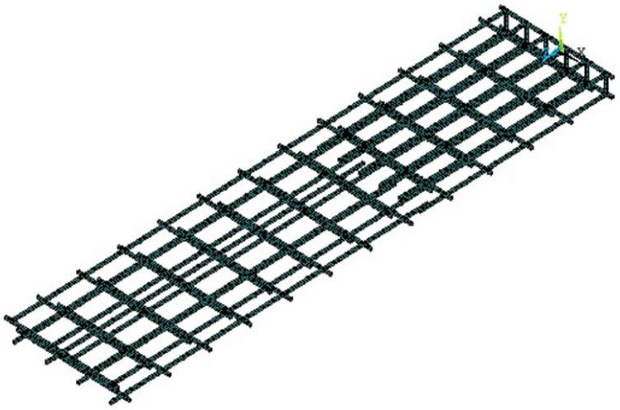

Fig. 5: Steel reinforcement bars meshing for all slabs

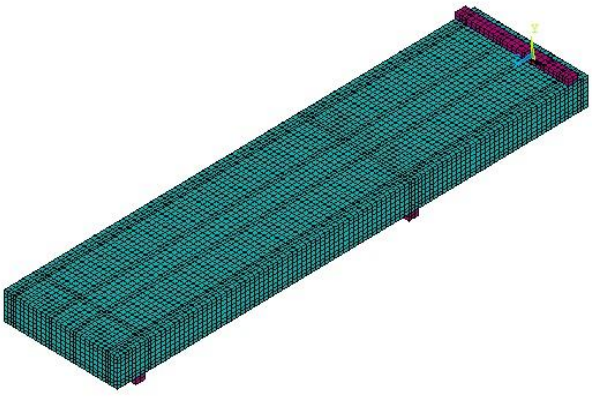

Fig. 6: Concrete meshing of all slabs

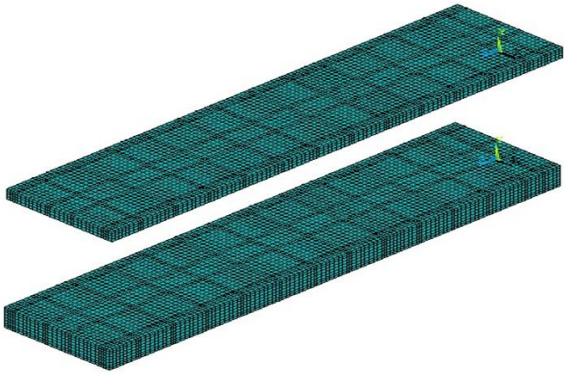

Fig. 7: Concrete meshing of slabs S-2 and S-3

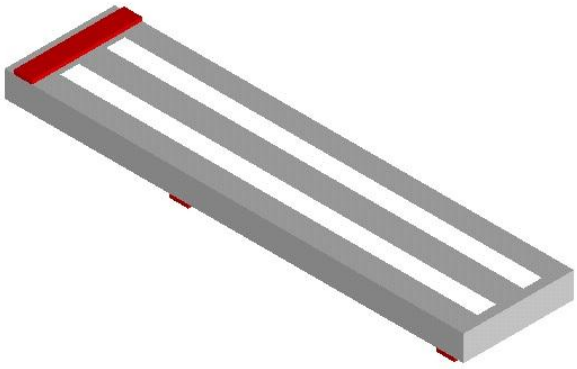

Fig. 8: GFRP strips meshing of slabs S-4 and S-5

VI. NON-LINEAR SOLUTION

The Full Newton-Raphson method is adopted to solve the set of nonlinear equations, with a sufficiently large number of solution sub-steps during the loading process to capture the different stages of the behavior, such as cracking, yielding, and failure. The equation solvers is sparse direct. The automatic time stepping, which regulates the sub-step size according to the convergence of the solution, is activated to help reduce computational time. For Solid 65 element, 185 brick element, a 2 x 2 x 2 set of Gaussian integration points is used. A convergence tolerance of 5% or 10% is assumed based on the displacement degree of freedom or force.

VII. MODELING OF DEBONDING

Modeling of the debonding phenomenon in adhered materials requires appropriate knowledge of the behavior of each bonded component as well as the interaction between the bonded parts. In the experimental program, three tested cantilever slabs failed by debonding: two of the slabs were strengthened with GFRP layers and one slab was strengthened with steel plate strips.

For the slabs S-4 and S-5 which strengthened with GFRP layers, debonding occurred along the adhesive-concrete interface. The debonding initiated from loading locations till the maximum negative moment (above roller support). For the slab S-6 which strengthened with steel plates, the plates debonded along adhesive of interface with concrete surface. Debonding of the above specimens is included in the developed FE models by using the cohesive zone material CZM.

A cohesive zone material (CZM) model is required to define the traction-separation [(normal or shear stress)-(normal jump or tangential slip)] behavior along the interface. A bilinear CZM model, available in ANSYS, is used in this study. The model consists of a linear elastic portion until a maximum normal (peeling) or shear stress is reached, and a softening line, that ends at the maximum normal jump or tangential slip [10].

Fig.9 shows a typical bilinear CZM model, in which six parameters are needed to define the model. For debonding induced by normal stresses, the parameters are: σ_{max}

ISSN: 2277-3754
ISO 9001:2008 Certified
International Journal of Engineering and Innovative Technology (IJEIT)
Volume 7, Issue 6, December 2017

(maximum normal stress), un* (normal jump accompanying max σ_{max}), and unc (normal jump at completion of debonding). While for debonding caused by shear stresses, the parameters are: τ_{max} (maximum stress), δ_t* (tangential slip accompanying τ_{max}), and δ_t^c (tangential slip at completion of debonding).

The shear debonding parameters were clarified as follows [10]:

$$\tau_{max} = 1.5\beta_w f_t \quad (1)$$

$$\beta_w = \sqrt{\frac{2.25 - (b_f/b_c)}{1.25 + (b_f/b_c)}} \quad (2)$$

$$f_t = 0.56\sqrt{f_c'} \quad (3)$$

Where:
β_w : Width ratio
f_t : Concrete tensile strength
b_f : Width of GFRP laminate (mm)
b_c : Center to center of strips (mm)
f_c': Concrete compressive strength (N/mm^2)

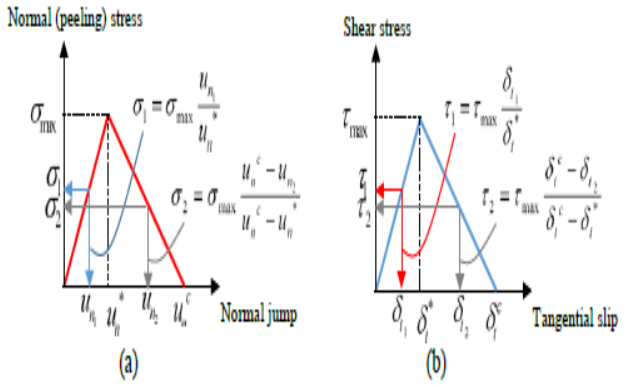

Fig. 9: Bilinear CZM model a) normal debonding and b) shear debonding [10]

VIII. RESULTS AND DISCUSSION

A. Load-deflection behavior

The deformation shape of all cantilever slabs simulated from fig. 10 to fig. 16. The load-deflection behavior showed from fig. 17 to Fig. 23 under applied load as a comparison between experimental and finite element (F.E) results for reinforced concrete cantilever slabs. In general, finite element of slabs shows the good agreement with experimental results for crack load, yield load and ultimate load. There are a deference of stiffness in the first part of load-deflection behavior for all finite elements compared with experimental load-deflection behavior. The first part of load-deflection behavior for all finite element slabs is more stiffness than experimental behavior due to exposure the experimental specimens to duplicate the loading systems. The failure load obtained from the analysis is in good agreement with the experimental failure load, with the difference between FE and experimental ultimate loads range between 3.46% and 21%. The comparisons of load-deflection behavior at mid-span were presented from fig. 24 to fig. 30. It's showed a good agreement between FE model results and experimental results. It can be notice that the deflection values of FE models is lower than the experimental results.

B. Strain distributions

The strains of steel reinforcement bars and GFRP laminates as experimental and FE results were shown from fig. 31 to fig. 43. The difference ratios of the yield load between FE models results and experimental results were ranged from 0% to 24%. This results show a good agreement compared with experimental results.

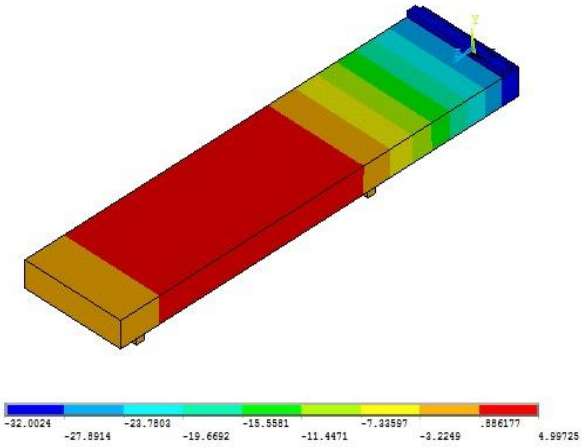

Fig. 10: Deformation shape of control slab S-1

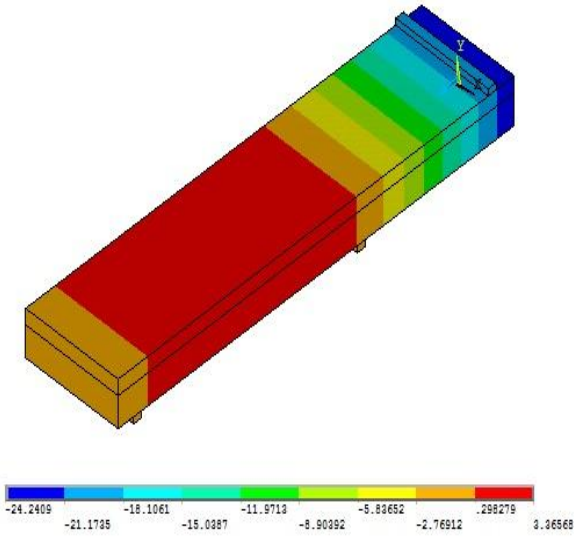

Fig. 11: Deformation shape of slab S-2

ISSN: 2277-3754
ISO 9001:2008 Certified
International Journal of Engineering and Innovative Technology (IJEIT)
Volume 7, Issue 6, December 2017

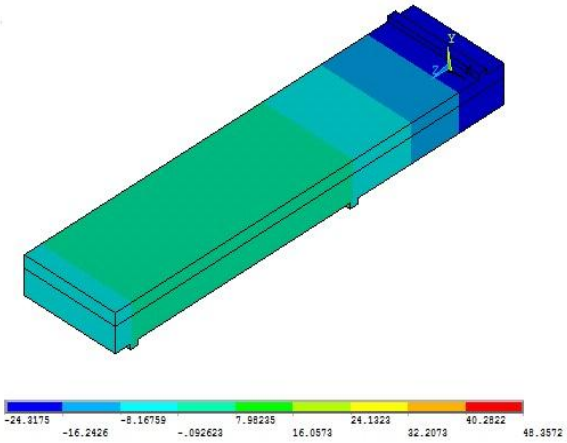

Fig. 12: Deformation shape of slab S-3

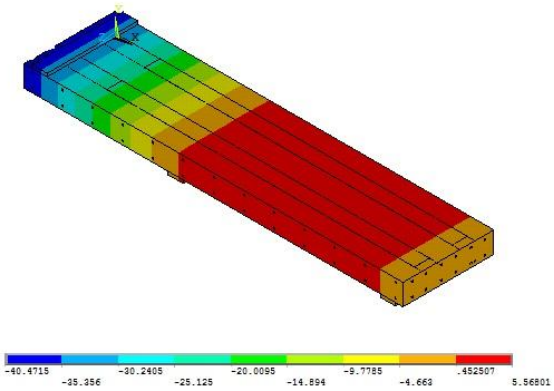

Fig. 13: Deformation shape of slab S-4

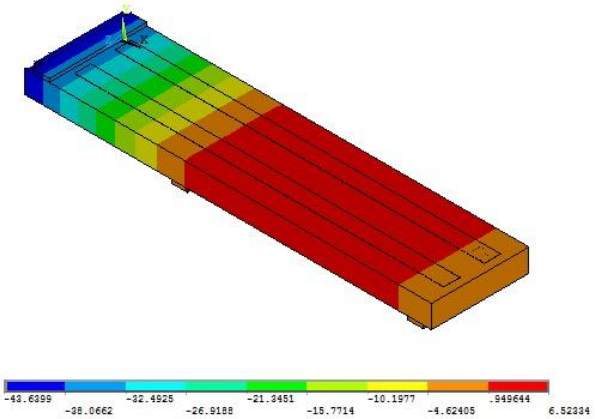

Fig. 14: Deformation shape of slab S-5

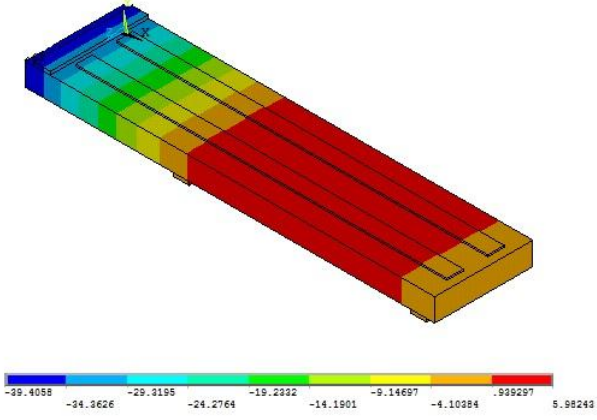

Fig. 15: Deformation shape of slab S-6

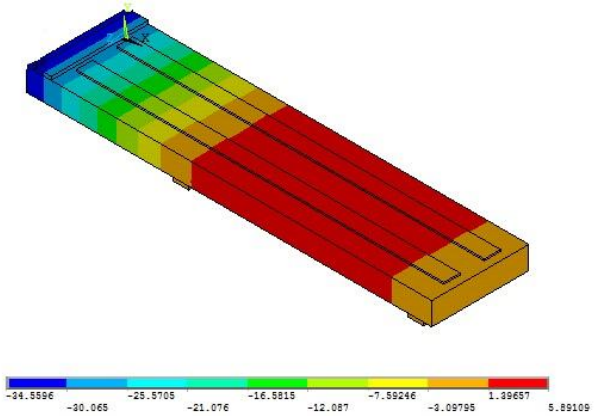

Fig. 16: Deformation shape of slab S-7

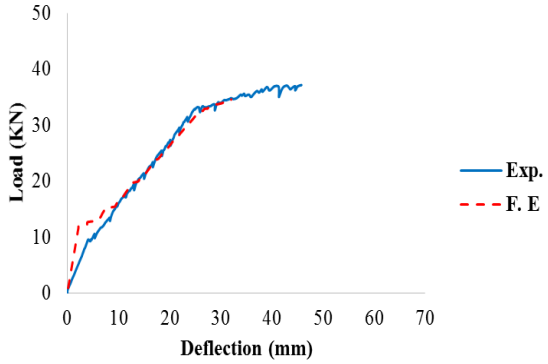

Fig. 17: Load-deflection of slab S-1 under applied load

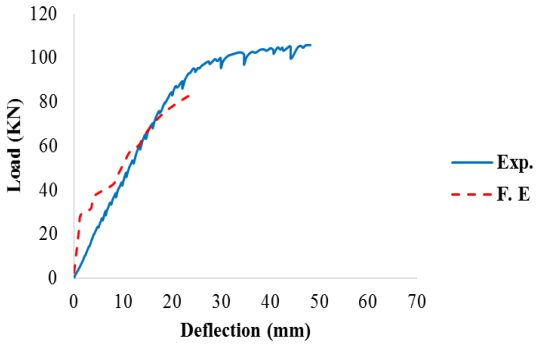

Fig. 18: Load-deflection of slab S-2 under applied load

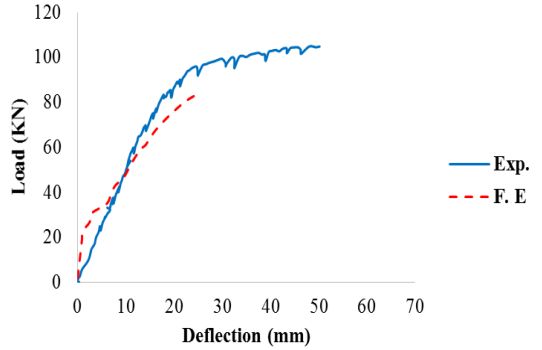

Fig. 19: Load-deflection of slab S-3 under applied load

ISSN: 2277-3754
ISO 9001:2008 Certified
International Journal of Engineering and Innovative Technology (IJEIT)
Volume 7, Issue 6, December 2017

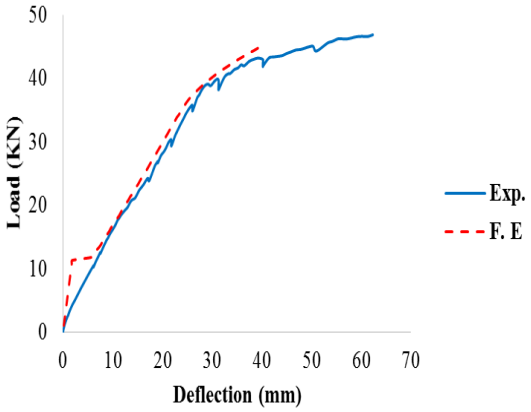

Fig. 20: Load-deflection of slab S-4 under applied load

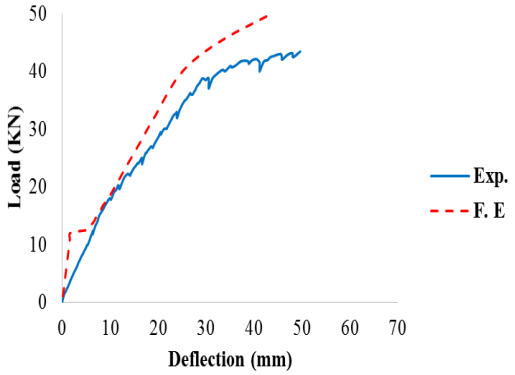

Fig. 21: Load-deflection of slab S-5 under applied load

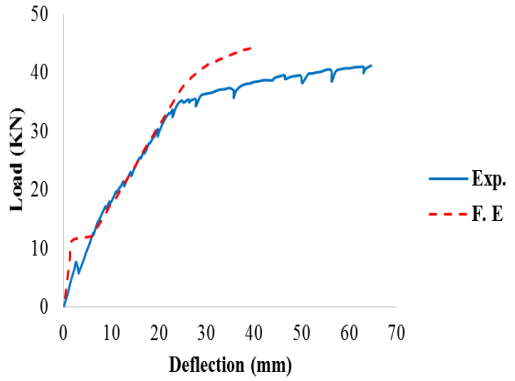

Fig. 22: Load-deflection of slab S-6 under applied load

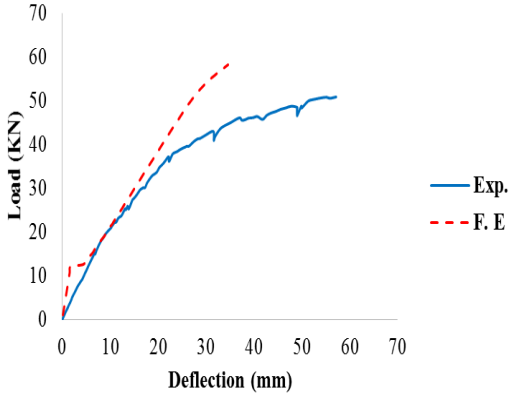

Fig. 23: Load-deflection of slab S-7 under applied load

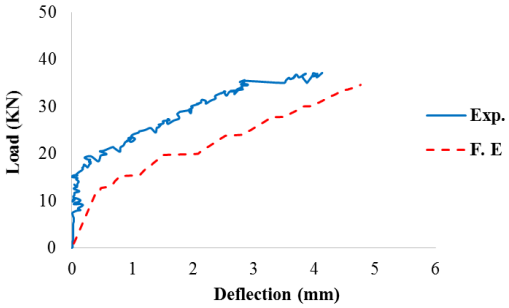

Fig. 24: Load-deflection of slab S-1 at mid-span

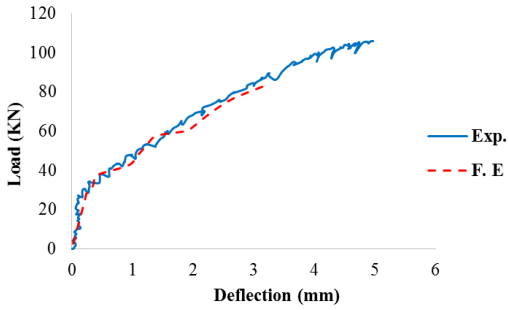

Fig. 25: Load-deflection of slab S-2 at mid-span

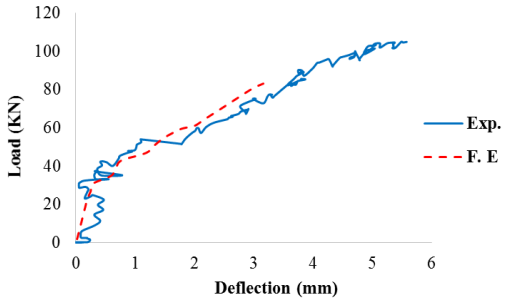

Fig. 26: Load-deflection of slab S-3 at mid-span

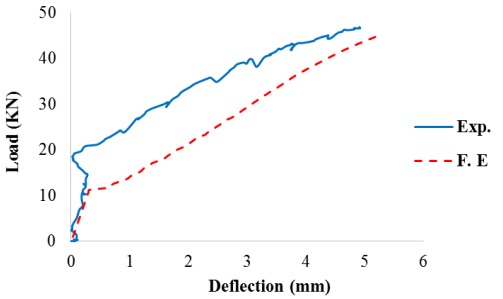

Fig. 27: Load-deflection of slab S-4 at mid-span

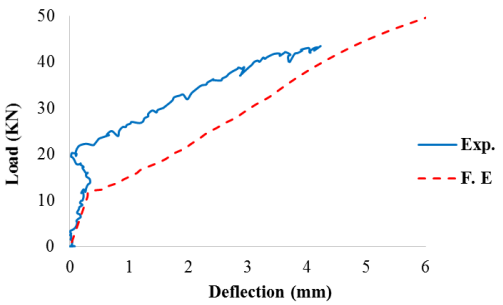

Fig. 28: Load-deflection of slab S-5 at mid-span

ISSN: 2277-3754
ISO 9001:2008 Certified
International Journal of Engineering and Innovative Technology (IJEIT)
Volume 7, Issue 6, December 2017

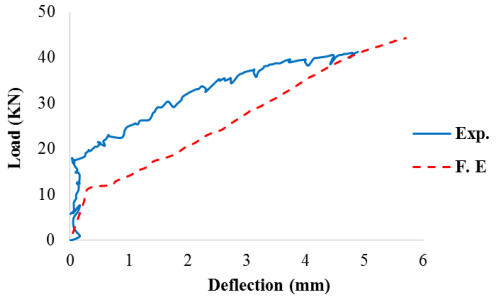

Fig. 29: Load-deflection of slab S-6 at mid-span

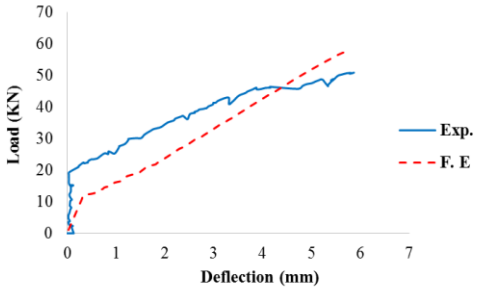

Fig. 30: Load-deflection of slab S-7 at mid-span

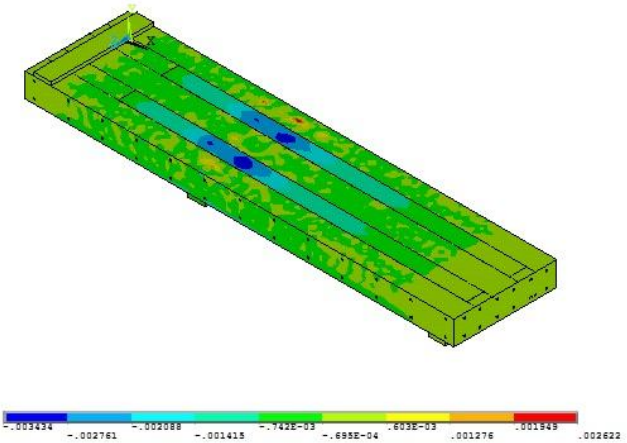

Fig. 31: Strain distribution of GFRP of slab S-4

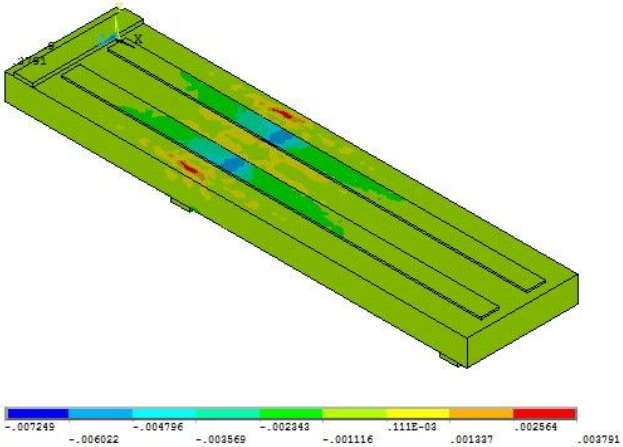

Fig. 32: Strain distribution of steel plates of slab S-6

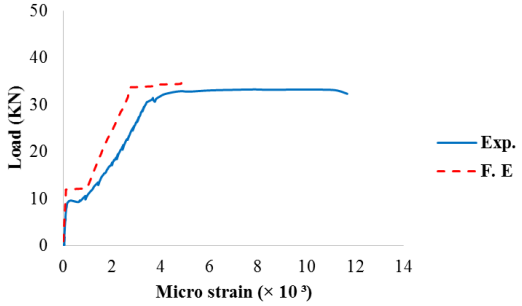

Fig. 33: Load-strain of steel of control slab S-1

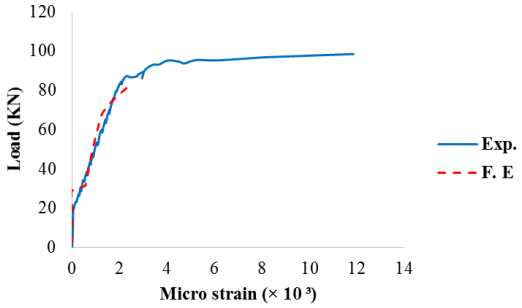

Fig. 34: Load-strain of old steel for slab S-2

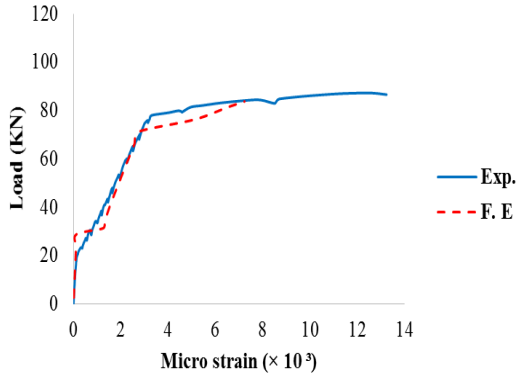

Fig. 35: Load-strain of new steel for slab S-2

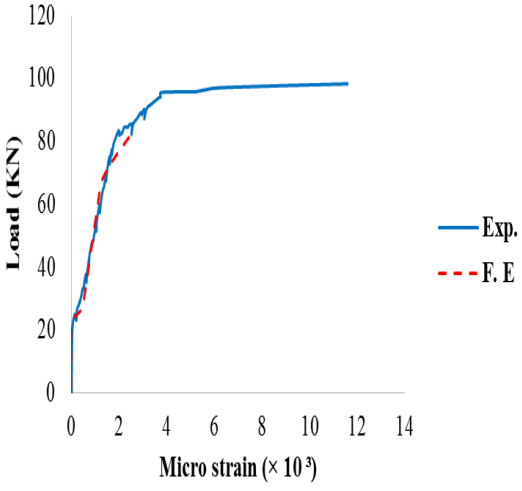

Fig. 36: Load-strain of old steel for slab S-3

ISSN: 2277-3754
ISO 9001:2008 Certified
International Journal of Engineering and Innovative Technology (IJEIT)
Volume 7, Issue 6, December 2017

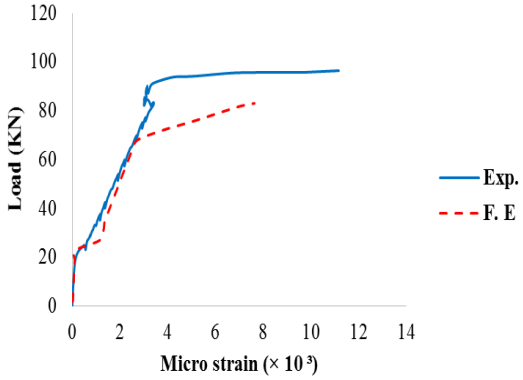

Fig. 37: Load-strain of new steel for slab S-3

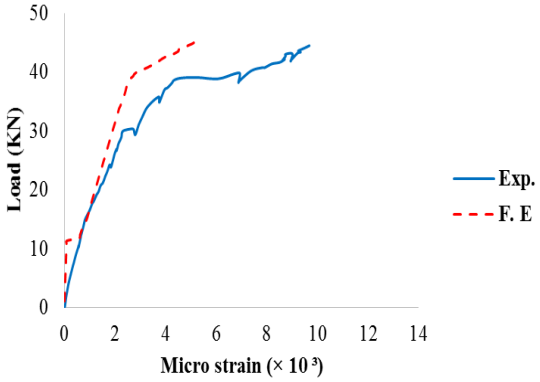

Fig. 38: Load-strain of steel of slab S-4

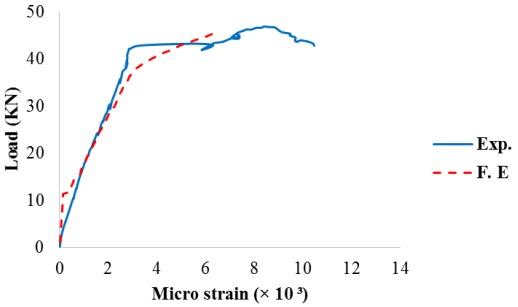

Fig. 39: Load-strain of GFRP of slab S-4

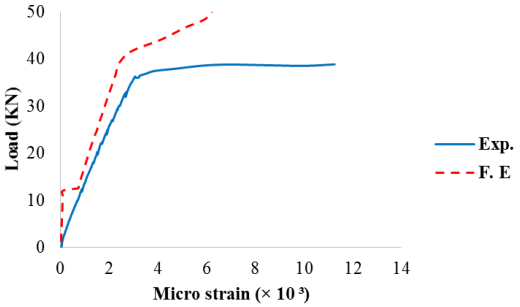

Fig. 40: Load-strain of steel of slab S-5

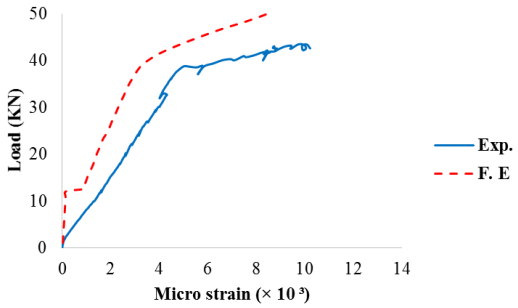

Fig. 41: Load-strain of GFRP of slab S-5

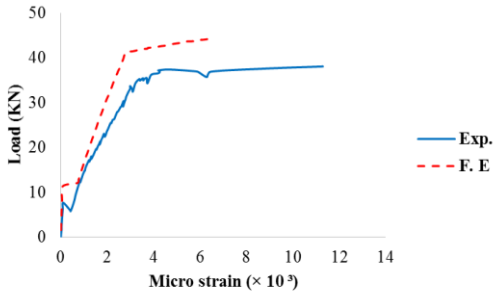

Fig. 42: Load-strain of steel bars of slab S-6

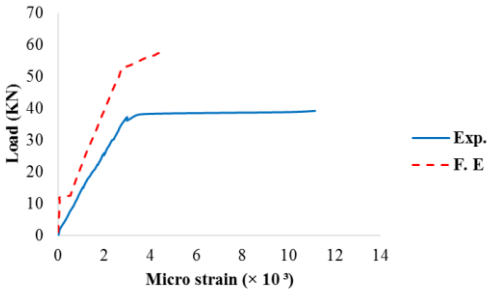

Fig. 43: Load-strain of steel bars of slab S-7

Table 3: Comparisons between experimental and finite element model results

Samples No.	Crack load (kN)			Yield load (kN)			Ultimate load (kN)		
	Exp.	F.E	Exp. / F.E	Exp.	F.E	Exp. / F.E	Exp.	F.E	Exp. / F.E
S-1	9.65	11.70	0.82	30.06	33.76	0.89	37.16	34.58	1.07
S-2	23.77	28.75	0.83	78.02	71.25	1.10	105.85	83.75	1.26
S-3	24.89	22.90	1.09	82.41	68.06	1.21	104.84	83.06	1.26
S-4	15.00	11.25	1.33	38.66	38.75	1.00	46.88	45.26	1.04
S-5	12.00	12.00	1.00	35.57	39.19	0.91	43.47	50.01	0.87
S-6	15.45	11.30	1.37	33.06	41.00	0.81	41.22	44.3	0.93
S-7	17.96	12.00	1.50	36.15	52.64	0.69	50.88	58.26	0.87

ISSN: 2277-3754
ISO 9001:2008 Certified
International Journal of Engineering and Innovative Technology (IJEIT)
Volume 7, Issue 6, December 2017

A. Comparisons between experimental and F.E results

Table 3 shows the different ratios of the crack load between experimental results and F.E of all slabs were ranged between 0% and 33% fig. 44. While the different ratios of the yield load were found to be 0.2% till 45% fig. 45. The different ratios were from 3.5% to 21% for ultimate load of slabs fig. 46.

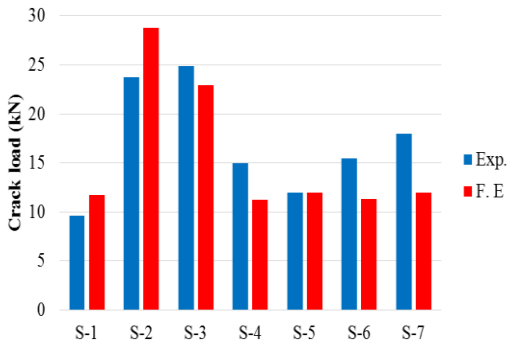

Fig. 44: Comparison of crack load between Exp. and F.E

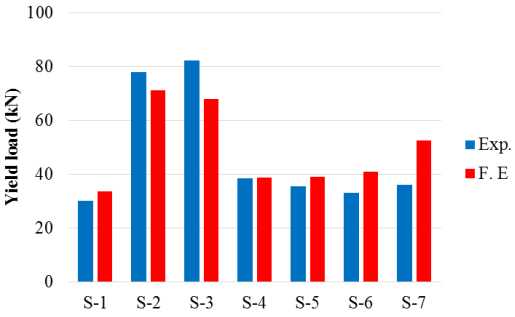

Fig. 45: Comparison of yield load between Exp. and F.E

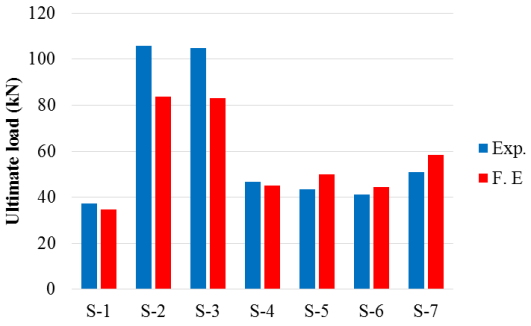

Fig. 46: Comparison of ultimate load between experimental and F.E

IX. CONCLUSION

There is a good agreement between FE predictions and experimental results when comparing the load-deflection. The steel plates never recorded any strain results from finite element model such as experimental results. The deflection under applied load of all strengthened slabs of finite element models are not larger than the experimental results. The strain of GFRP layers shows a good predict compared with experimental results.

REFERENCES

[1] B. B. Adhikary, H. Mutsuyoshi, and M. Sano, "Shear strengthening of reinforced concrete beams using steel plates bonded on beam web: experiments and analysis," Construction and Building materials, vol. 14, pp. 237-244, 2000.

[2] X. Lu, L. Ye, J. Teng, and J. Jiang, "Meso-scale finite element model for FRP sheets/plates bonded to concrete," Engineering structures, vol. 27, pp. 564-575, 2005.

[3] J.-G. Park, K.-M. Lee, H.-M. Shin, and Y.-J. Park, "Nonlinear analysis of RC beams strengthened by externally bonded plates," Computers and Concrete, vol. 4, pp. 119-134, 2007.

[4] X. Teng and Y. Zhang, "Nonlinear finite element analyses of FRP-strengthened reinforced concrete slabs using a new layered composite plate element," Composite Structures, vol. 114, pp. 20-29, 2014.

[5] B. Perumalsamy, N. Antonio and G. James, FRP Composites for Reinforced and Prestressed Concrete Structures'', New York-USA: Taylor & Francis, 2009.

[6] "ES 4756-1/2013, Egyptian Standard Specification "Cement - Part 1 Composition, Specification and Conformity Criteria for Common Cement"," Housing and Building Researching Center, Control, Egyptian Organization for Standard and Quality, Cairo-Egypt, 2013.

[7] "ES 1109/2002, Egyptian Standard "Aggregates for Concrete"," Housing and Building Research Center, Control, Egyptian Organization for Standard and Quality, Cairo-Egypt, 2002.

[8] "ECP 203-2009 Egyptian Code of Practice for Design and Construction of Concrete Structures Code, Standing Committee to prepare the Egyptian," HBRC, Cairo-Egypt, 2009.

[9] ANSYS R15.0, "Release 14.5 Documentation for ANSYS," in ANSYS, 15.0 ed. Canonsburg, PA, USA, 2015.

[10] A. R. Jawdhari, "Behavior of RC beams strengthened in flexure with spliced CFRP rod panels," 2016.